T Barbui et al.

Radiative edge cooling experiments in Wendelstein 7-X startup limiter campaign

Radiative edge cooling experiments in Wendelstein 7-X start-up limiter campaign

T. Barbui[1], F. Effenberg[1], R. König[2], M. Krychowiak[2], O. Schmitz[1], J. Baldzuhn[2], B. D. Blackwell[3], P. Drews[4], Y. Feng[2], M. Jakubowski[2], S. Kwak[2], Y. Liang[4], S. Liu[4], H. Niemann[2], T. Sunn Pedersen[2], J. Svensson[2], D. Zhang[2] and the W7-X Team[2]

[1] Department of Engineering Physics, University of Wisconsin-Madison, Madison, WI 53706, USA
[2] Max-Planck-Institut für Plasmaphysik, 17491 Greifswald, Germany
[3] Plasma Research Laboratory, Research School of Physics and Engineering, Australian National University, Canberra, ACT 0200 Australia
[4] Forschungszentrum Jülich GmbH, Institut für Energie- und Klimaforschung - Plasmaphysik, Partner of the Trilateral Euregio Cluster (TEC), 52425 Jülich, Germany

E-mail: barbui@wisc.edu

Abstract. Impurity seeding experiments during the start-up limiter campaign of Wendelstein 7-X provide first evidence for a localization effect of the three-dimensional magnetic edge structure on the seeded impurities and their radiation distribution and cooling effect. Moreover, species dependencies have been seen. Nitrogen was observed to cool the entire edge plasma, with a stronger electron temperature reduction measured at the downstream position at the limiter. The radiation was limited at the periphery of the confined region. Both the T_e reduction and the radiation enhancement were directly correlated to the injection of the coolant gas. Mitigation of the limiter heat loads was also measured. Neon was observed to radiate in the confined plasma region, continuing long after the end of the injection and cooling the entire plasma.

Introduction

The new optimized helical advanced stellarator device Wendelstein 7-X (W7-X) started its first plasma operation (OP1.1) in a limiter configuration [1][2]. The last closed flux surface (LCFS) of the plasma was defined by 5 poloidal uncooled graphite limiters [3]. In this initial campaign, besides the commissioning of the main device systems and diagnostics required for the next divertor campaign [4][5][6], it was also possible to perform first physics experiments. Among those was the cooling of the edge plasma by impurity seeding of nitrogen (N_2) and neon (Ne). These experiments aimed to test the method in the specific scrape-off layer geometry of the W7-X limiter campaign and to provide first actual experiments of radiative edge cooling in stellarators in view of the island divertor phase of W7-X. This divertor concept will be used for the future quasi-steady-state operations and it is expected that the heat flux reaching the plasma facing components will be one of the major concerns for the successful operation of the device [7][8]. One possible method to reduce this heat flux is to use intrinsic and actively injected impurities species in the edge of the plasma to dissipate energy by impurity radiation. This method of radiative cooling of the plasma edge by impurity seeding has been extensively used in many devices to remove the heat from the divertor/edge plasma in order to protect the plasma facing components. As radiators, typically low charge state (Z) elements like neon (Ne), argon (Ar) or nitrogen (N) are used. Radiative edge cooling with such gas species has been investigated already in different tokamaks where, besides the purpose of radiative edge cooling, non-intrinsic seeded impurities have also been shown to be effective to mitigate ELMs and to facilitate the detachment [9][10][11][12]. For stellarator devices there is not yet a large experience, and for the island divertor specifically only very limited initial experiments were conducted in the short island divertor campaign at W7-AS. Only in the Large Helical Device (LHD) impurity seeding experiments were carried out. Here, Ne, N_2 and Kr were used as most effective species and enhancement of plasma radiation as well as reduction of the divertor heat load were observed without significant confinement degradation [13][14]. Ne was observed to radiate considerably from the core region in addition to the strong edge radiation, whereas N_2 was observed to radiate only from the peripheral region [15].

In this paper, we report on a first-time assessment of radiative edge cooling properties for the limiter start-up scenarios at W7-X. These experiments are unique in the sense that the 3D magnetic edge structure for this campaign was available for the first time in any stellarator device. In particular, the magnetic structure is nicely ordered into three separated magnetic flux bundles, which represent the helical scrape-off layer (SOL) in this configuration [16][17]. This setup hence bears unique opportunities to better understand the generic properties of impurity transport and radiation related to radiative edge cooling. Also, the setup enables for the first time to assess the interaction of a radiative mantle with the helically twisted, close fitting first wall at W7-X, which represents a mixture of first wall materials and might mandate cooling of the plasma boundary layer much before even considering heat flux tolerances for actively cooled components in the divertor. In the experiments considered here, Ne and N_2 were injected through a versatile piezo nozzle setup [6] located comparably close to the last closed flux surface (LCFS), about 18 cm away from it. The cooling effects on the plasma edge were measured by Langmuir probes [6] and a new thermal helium beam system [18]. The mitigation of the heat loads on the limiter were assessed by infra-red (IR) imaging spectroscopy of surface temperatures [26]. The poloidal radiated power distribution was measured by a bolometer array [27].

The first goal of these experiments was to demonstrate their feasibility by achieving and measuring the cooling effects. The second goal was to resolve in which region the cooling was dominant (scrape-off layer vs confinement) and to understand whether local or global cooling was predominant in the 3D scrape-off layer that characterizes the W7-X limiter scenario. These experiments were also useful in preparation for the foreseen feedback-controlled gas injection to be implemented for the next divertor campaigns. Such a system will be based on the control of the edge T_e/n_e or the edge impurity radiation by flow-controlled gas injection. These experiments as well as the extrapolation to the island divertor are based on an extensive numerical study of plasma edge transport and radiation cooling by intrinsic and seeded impurities carried out with the fully 3D fluid plasma edge and kinetic neutral transport code EMC3-EIRENE [16]. These simulations predict that N_2 seeding enables to actively cool the plasma edge with small penetration in the core plasma, while Ne results in a deeper expansion towards the core of the radiation region. Also, the modelling results predict a localization of the seeded impurities aligned with the magnetic structure. These predictions represent a valuable guideline for the experiments and they will be discussed in the last chapter.

Description of the experiment

The Wendelstein 7-X stellarator (W7-X)
W7-X is the largest fully optimized, super-conducting stellarator in the world with a minor radius of 0.5 m, major radius of 5.5 m and magnetic field strength on axis $B = 2.5$ T. W7-X is a HELIcal Advanced Stellarator (HELIAS) with strongly varying plasma cross-section, five field periods and low shear. The device consists of five nominally identical modules. Each of these is made of two flip-symmetric parts, so that in fact the device is composed of ten almost identical half-modules [18]. The poloidal symmetry plane changes within a half-module from a bean-shaped cross-section at $\phi_{tor}=0°$ through a tear-shape cross-section at $\phi_{tor}=12.3°$ to a triangular cross-section at $\phi_{tor}=36°$ [20].

For the start-up campaign five poloidal graphite limiters were installed on the torus inboard side, which defined the plasma boundary and avoided significant power loads to the metallic in-vessel components [3]. For the later operation phases, the heat fluxes will be distributed over a much larger area provided by the divertor target plates in the island divertor, where pumping will also be implemented [21].

The localization of the limiters within the helicity of the plasma equilibrium and the local magnetic shear at the plasma boundary establishes a 3D boundary consisting of three distinct types of magnetic flux tubes with different target-to-target connection lengths (L_C) (36, 43, 79 m) [16].

Two different magnetic configurations were used during the seeding discharges: the standard OP1.1 configuration and a configuration at increased rotational transform, measured by the iota ($i=2\pi·d\psi_\theta/d\psi_\varphi$). In the standard OP1.1 configuration the 5/6 island chain is slightly inside the LCFS and the 5/5 islands, which later will establish the island divertor, are far outside of the LCFS such that no large islands are present close to the limiter. Hence, no direct heat and particle loads connected to the interaction of the islands are expected [5]. In the increased iota OP1.1 configuration the 5/5 islands move inwards and become visible in the far SOL. The 5/6 island, located

inside of the last closed flux surface, is moved inwards too and is now located in the particle source region, thus interacting with the recycling flux as main plasma particle source [22]. The plasma heating is provided in this initial phase only by electron cyclotron resonance heating (ECRH) with 6 gyrotrons, delivering a maximum power of 4.3 MW. For the experiments described in this work the input power was set to 2-3 MW and the central plasma parameters were $T_e \sim 5$ keV, $n_e \sim 2\times10^{19}$ m^{-2}.

Injection system and edge diagnostics
Figure 1 shows the position of the diagnostics used with respect to the magnetic flux tube structure. The pentagon shape of the torus is clearly visible. Machine module 1 is the upper right one, then the others follow anti-clockwise. In the bean-shaped cross-section of each module, on the inboard side, a limiter is installed.

The impurities are seeded by gas injection from one of the two gas boxes installed in the device [6]. The gas boxes are located in two symmetric positions, one at the bottom of the tear-shape cross-section in module 3 and one at the top of the same cross-section in module 5 as shown in Figure 1. Nitrogen is injected from the gas box in module 3, while neon from the one in module 5. The two locations are connected by the same flux tube and they lie in an upstream position with respect to the limiter target. The gas is injected through a fast piezo valve (opening time of few ms) [23], which enables fast duty cycles for the gas injection and a direct control of the amount of gas utilized. In the experiments under consideration here, the impurity seeding is provided by one single source. The same arrangement will be also used during the first divertor campaigns (OP1.2). In the later divertor phase (OP2) 10 toroidally symmetric gas boxes are envisaged, two in each module in the upper and lower divertor plate. Their aim is to provide a uniform cooling of the entire SOL and uniform fueling capabilities. In the experiments described in this paper, a first exploration of the seeding capabilities in the 3D plasm edge of W7-X is presented.

Three edge diagnostics were employed as main diagnostics to measure the variation of T_e in different locations within the SOL: the thermal He-beam and the Langmuir probe on the multi-purpose manipulator, located in two different upstream positions, and the Langmuir probes on two limiter tiles, at the downstream target position.

The He-beam measures radial profiles of T_e and n_e through line-ratio spectroscopy on thermal He [24]. The gas is injected through the gas box in module 5. This gas box is equipped with a thin capillary nozzle for small divergence beam. The He-beam diagnostic was originally designed to measure T_e and n_e in the SOL along 8 lines-of-sight (LoS) perpendicular to the beam propagation, with 1 cm spatial resolution in the radial direction [18]. However, due to unfavorable coating of the observation window originating from the plasma operation, only spatially averaged temperatures and densities were obtained. Time resolution is 25 ms [18].

The multi-purpose manipulator is installed at the outboard side of the tear-shape cross-section in module 4 as shown in figure 1. In this initial phase the manipulator was equipped with the so-called combined probe, which includes five Langmuir probe pins [25]. With the manipulator in a fixed position within the SOL, time traces of temperature and density are measured. In the experiments presented here the manipulator was parked ~7cm outside the LCFS providing temperature and density measurements with a time resolution of 0.2 ms.

The limiter Langmuir probes comprise two arrays with 20 probes each installed in two tiles of the limiter in module 5 (one upper and one lower with respect to the mid plane). The probes provide radial profiles of T_e and n_e from the LCFS to 5 cm in the SOL with a 2 ms time resolution [6].

In Figure 1 are shown the magnetic field lines in the SOL for the flux tube which is fuelled by the N$_2$ injection. Such a tube connects the N$_2$ puff location with the He-beam position and the Langmuir probe at the midplane. Hence the He-beam and the upstream Langmuir probe lie on a flux tube that is directly fuelled by the N$_2$ injection, whereas the limiter equipped with the Langmuir probes intercepts a flux tube which is not directly in the injection cloud of the gas inlet. This is true for both magnetic configurations used during these impurity seeded experiments. In the standard OP1.1 magnetic configuration the N$_2$ valve fuels the long L_C flux tube (79 m) and both the He-beam and the upstream Langmuir probe are located in this flux tube. In the increased iota OP1.1 configuration the N$_2$ source fuels the 5/5 island in the far SOL and the long L_C flux tube. In this configuration the He-beam is predominantly in the long L_C flux tube while the upstream Langmuir probe sits inside the island. He-beam and upstream Langmuir probe thus provide measurements of local cooling effects in the 3D helical SOL topology of the W7-X limiter plasmas. The cooling observed on the limiter tiles is instead due to cross-field transport between different flux tubes and its measurements are an indicator of global cooling effects in the SOL.

Neon is puffed in through the He-beam gas box, fuelling the same flux tube as for nitrogen. In the Ne experiments however only the downstream measurements from the limiter Langmuir probes are available.

Additionally, the surface temperature of the limiter 5 is monitored by an infrared camera. The camera is a microbolometric camera (observable wavelength range 8-14 μm, spatial resolution ~5 mm, frame rate 50 Hz). From the surface temperature data the heat flux density is evaluated by solving a one-dimensional heat diffusion equation for bulk graphite material [26].
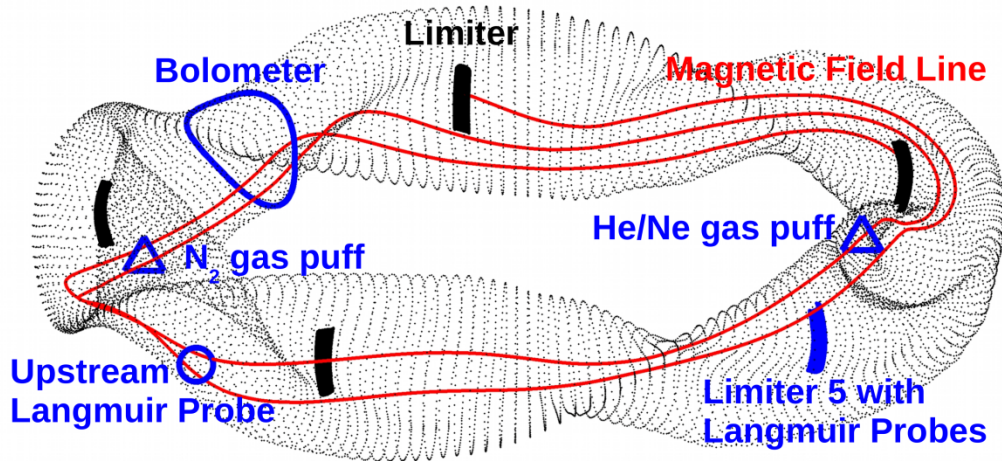

Figure 1. Field line trajectories in the scrape-off layer to show the position of the diagnostics used with respect to the magnetic flux tube structure. He-beam and upstream Langmuir probe lie on flux tubes that are directly fuelled by the N_2/Ne puff, while the limiter Langmuir probes are not connected to these flux bundles.

Finally, a two-camera bolometer system comprising a horizontal one with 32 channels and a vertical one with 40 channels with lines of sight covering the entire triangular cross section, allowing to measure the plasma radiation horizontally and vertically [27]. The tomographic inversion of the bolometer integrated signals is also performed leading to a 2D poloidal distribution of the plasma emissivity. This shows the regions where the impurities (intrinsic and extrinsic) mainly accumulate and radiate and will then be compared with the results of EMC3-EIRENE calculations.

Analysis of N_2 seeded discharges

N_2 seeding experiments were carried out injecting gas at different reservoir pressures: 100, 200, 300, 500 mbar, which yields different injection particle fluxes of 2×10^{19}, 4×10^{19}, 6×10^{19}, 1×10^{20} particles/s respectively. Effective cooling of the edge avoiding core contamination and consequent radiation collapse is found to be attainable at 300 mbar reservoir pressure.

Figure 2 presents an overview plot of the main plasma parameters during one of the N_2 seeding discharges at 300 mbar reservoir pressure. Time traces of heating power (a), electron temperature (b), electron density (c), diamagnetic energy (d), bremsstrahlung emission (e) and total radiated power (f) are shown. Heating power from ECRH was kept constant at ~3MW during the whole discharge. The gas injection is switched on after 100 ms from the start of the ECRH heating and it lasts for 200 ms. No significant effects of the injected impurities on the core T_e were observed, which remains constant at 6 keV for the whole discharge, whereas the temperature in the outer region ($0.82>r/a>0.54$) decreases during the gas injection by ~200 eV. This is a good indicator of a cooling limited to the external regions of the plasma with small impurity penetration in the inner core. Line-integrated density increases mainly due to wall outgassing and to some extend also due to the contribution of the electrons coming

from the ionization of N and N_2. Taking the total injected particle number, ignoring the implantation of N into plasma facing components and the pumping effect, and assuming full ionization and homogeneous distribution along the whole plasma volume, the maximum density increase due to nitrogen would be of 5.6×10^{18} m^{-3}. Hence we conclude that most of the density drive is born from an uncontrolled neutral source from wall outgassing. This is also supported by the fact that reference discharges without gas injection feature a very comparable density time trace. Diamagnetic energy does not reduce due to the injection indicating no core degradation. Bremsstrahlung emission is enhanced of a factor 2.4: considering that n_e increases by a factor 1.8 and T_e remains constant this implies that Z_{eff} decreases. The total radiated power increases significantly as a result of the injection, reaching 40% of the input power.
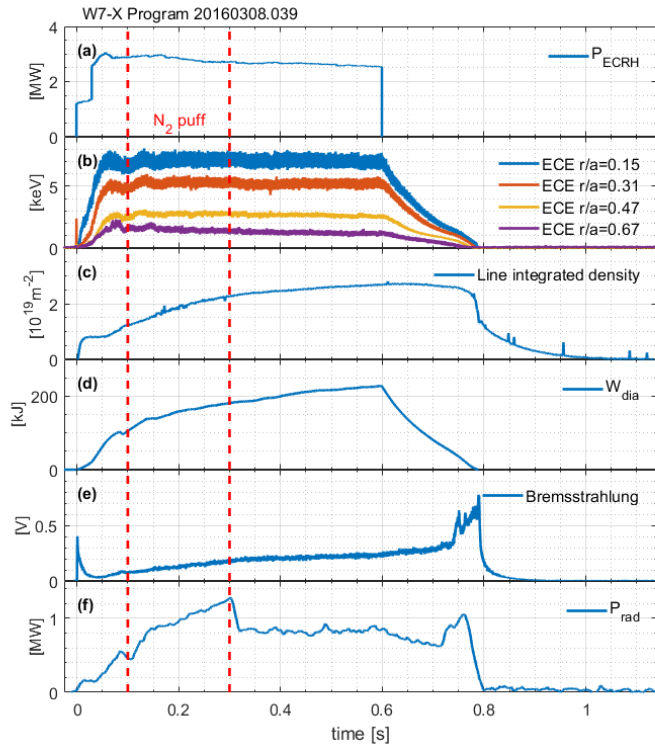

Figure 2. Overview plot of a discharge with N_2 gas injection. From top to bottom: (a) ECRH heating power, (b) electron temperature from the Electron Cyclotron Emission diagnostic (ECE), (c) line-integrated electron density, (d) diamagnetic energy, (e) bremsstrahlung emission, (f) total radiated power.
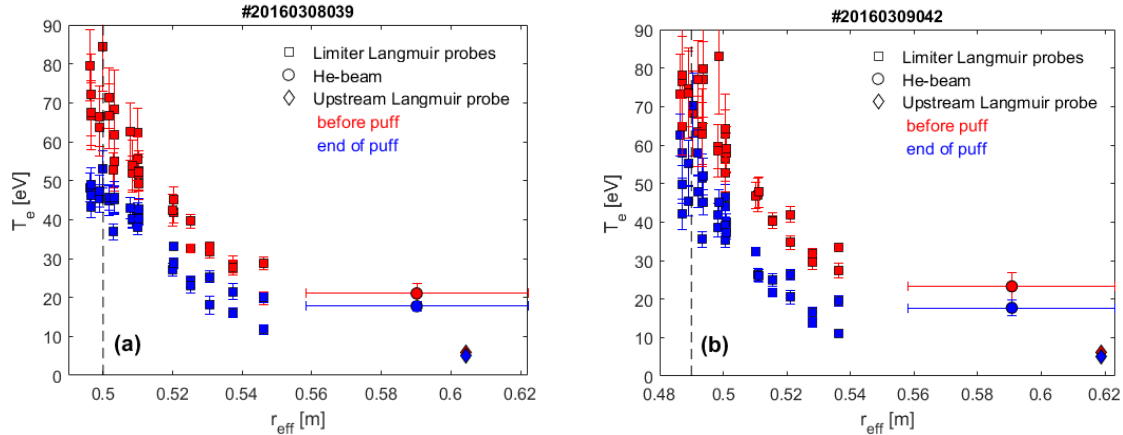
Figure 3. Radial profiles of the SOL temperature obtained combining the measurements from the three edge diagnostics (limiter Langmuir probes, He-beam and upstream Langmuir probe). The profiles are plotted before (red) and at the end (blue) of the N_2 injection. (a) refers to a discharge in the standard OP1.1 magnetic configuration. (b) refers to a discharge in the increased iota OP1.1 magnetic configuration. The LCFS for both configurations is shown as a dashed black line.

Figure 3 shows the variation of the radial profiles of the electron temperature $T_e(r_{eff})$ in the SOL following the N_2 gas injection. The profiles are obtained by combining the measurements of the three edge diagnostics as a function of r_{eff}. A clear reduction of T_e is seen in the whole radial length of the SOL as a consequence of the gas injection. The relative reduction depends, however, on the actual placing of the diagnostic in the flux tube geometry, especially with respect to the upstream/downstream locations.

He-beam and the upstream Langmuir probe both measure a decrease of the temperature of about 20%. The relative cooling detected by these two edge diagnostics is the same, which is consistent with the fact that they are located in the same flux tube directly fuelled by the nitrogen gas injection. This suggests that local cooling at the upstream position is homogeneous within a single flux tube. The absolute temperature measured by the upstream Langmuir probe is lower than the He-beam average value due to the fact that the probe is located farther outside in the SOL than the He-beam. Hence, the He-beam measurement averages over higher temperatures at smaller radii.

The mapping of the Langmuir probes data on the limiter shows an exponentially decaying profile into the SOL. The error bars are resulting from the fit to the exponential region in the I-V curve of the probes, which yields higher error bars for higher temperatures as the full electron saturation side cannot be reached with the sweep voltage available. There is a clear reduction of T_e outside of the error bars for both magnetic configuration due to the impurity injection. This reduction is seen in the region 2-5cm away from the LCFS. In the region closer to the LCFS, there is a clear trend downward in the measured T_e, although it stays within the increased error bars, still this is in line with an overall significant reduction of T_e due to the injection. The relative temperature reduction at the limiter (i.e. downstream) is about 30-40%, which is higher than at the upstream position of the He-beam and the upstream Langmuir probe. This means that cooling at the target, where flux tubes which are not directly fuelled by the N_2 injection intersect, is observed to be stronger than upstream cooling in the fuelled flux tube. Given that the gas injection is very localized in the 3D SOL structure of W7-X with limiters, a strong localization of the radiation from injected impurities was suspected. However, the results from the temperature measurements show that the injected impurities cool the plasma effectively also in regions which are not directly connected magnetically. This is most likely due to the nature of N_2 being a sticking gas species and hence, accumulation of injected gas on the limiter is likely, which will result in a local and gradually increasing N_2 source from the surface. Subsequent injections induce the mobilization of the nitrogen reservoir at the limiter, with consequent strong cooling in that location. This is the most likely reason for the effective and stronger cooling at the surface which is not directly connected to the injection flux tube. It was not possible to address the time dependence of this hypothesis because of the very limited experimental time (this experiment was performed in the very last week of the start-up campaign).
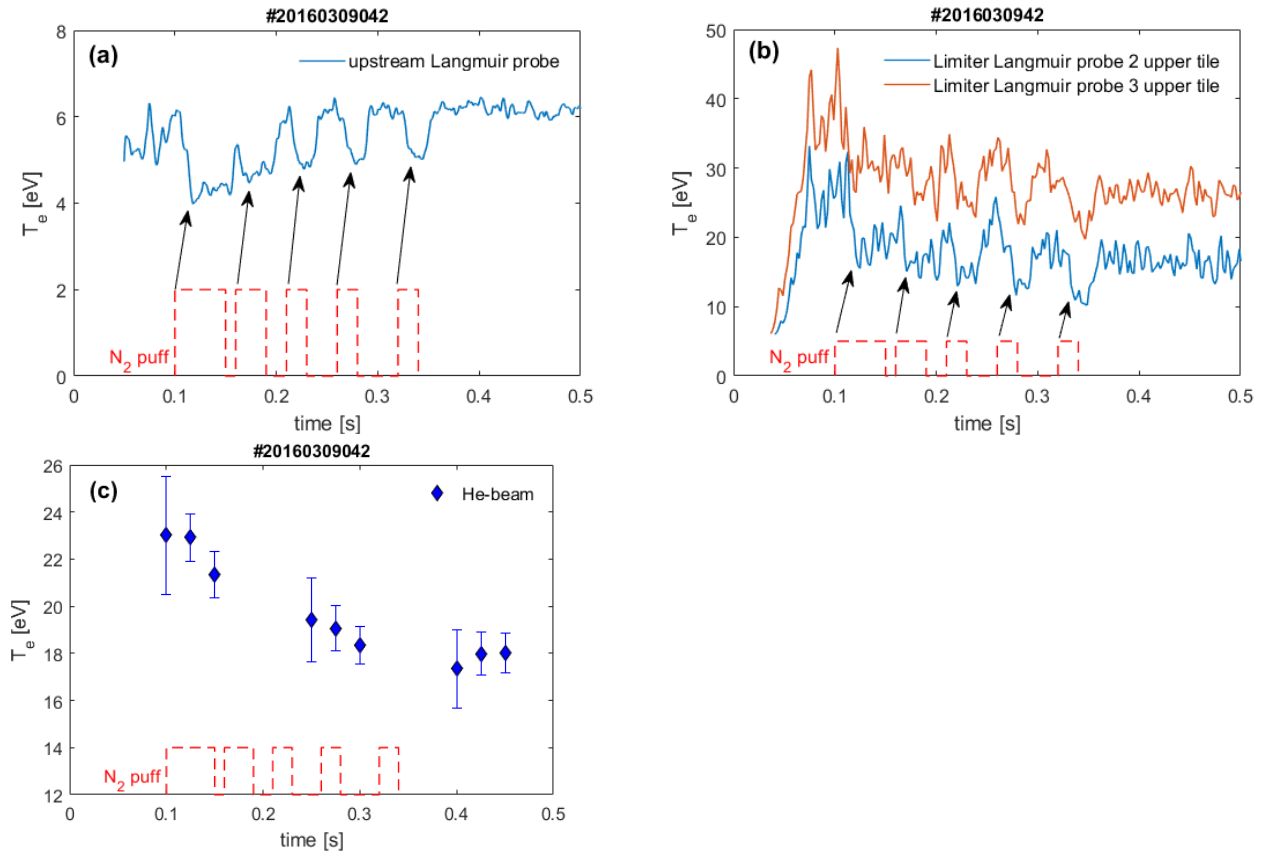
Figure 4. Pulsed N_2 injection. Time evolution of the electron temperature measured by (a) the upstream Langmuir probe, (b) two limiter Langmuir probes from the upper tile array (probe 2 at $r_{eff} = 0.536$ and probe 3 at $r_{eff} = 0.516$), (c) the He-beam.
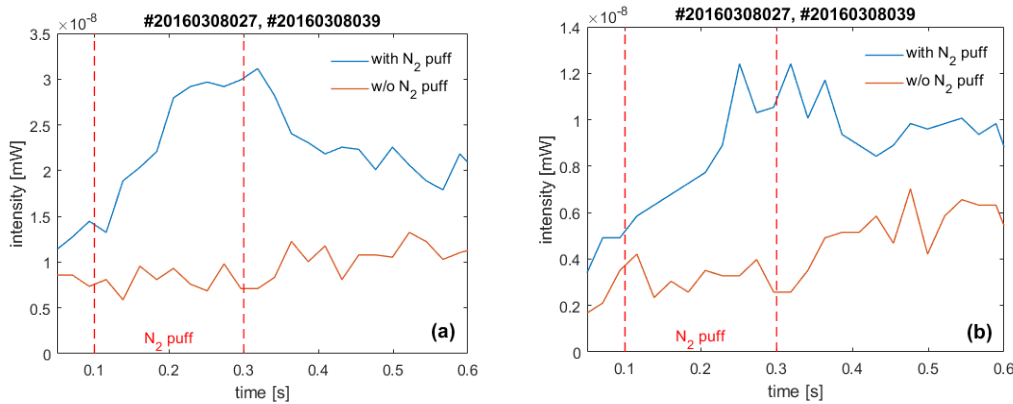

Figure 5. Line-integrated emissions from N I and N II measured by a central line-of-sight spectrometer at $\phi_{tor}=12.3°$. (a) N I 409.9 nm. (b) N II 399.5 nm.

One injection experiment was conducted with a pulsed N_2 gas injection to test the time response of the edge temperature. This experiment was conducted in the increased iota OP1.1 magnetic configuration. The results are presented in Figure 4, where the time traces of T_e are shown from the upstream Langmuir probe (Figure 4a), the limiter Langmuir probes (Figure 4b) and the He-beam (Figure 4c). The N_2 injection sequence is shown too and a

clear correlation between the injection time and the temperature variation is visible. Both the upstream Langmuir probe and the limiter Langmuir probes show a rapid drop of T_e soon after the opening of the valve and a recovery after the valve closes. The delay of ~5-10 ms between the time of the gas injection and the temperature response is mainly due to the valve opening time. The rapid response of the temperature variations shows that the dominant cooling action comes from the actively injected gas. The He-beam diagnostic has a long integration time (25 ms) and it was not synchronized with the valve opening, so it does not allow to resolve the injection oscillations. Nevertheless, also this measurement shows a clear gradual reduction of T_e indicating an accumulation of N_2 in the SOL yielding the overall edge cooling effect discussed before.

Limiter Langmuir probes and He-beam show a decay of the average temperature throughout the gas injection, which does not recover to its pre-injection level after the end of the injection. This because the SOL flux tubes are connected to the limiters, where an impurity source builds up during the gas injection and afterwards refills the flux tubes. Accumulation of N inside the SOL flux tubes is confirmed by visible spectroscopy. A single LoS spectrometer (Czerny-Turner, f_L 500 mm, spectral resolution 0.5 nm) observes the inner wall along the mid-plane of the device. Figure 5 shows that the emissions from atomic and low ionization stage of N remain high after the end of the gas injection, slowly decaying towards the end of the discharge, indicating a persistency of N in the SOL after the end of the injection.

The upstream Langmuir probe measures a full recovery of T_e immediately after the gas injection. In the high iota scenario the probe mounted on the mid-plane manipulator was parked in a far outwards position (see Figure 3b) where the 5/5 island is present. This magnetic island receives less impurities through limiter surface erosion compared to the SOL flux tubes, which are connected to the limiters and facing the confinement.

Analysis of Ne seeded discharges
Neon impurity seeding experiments were performed at reservoir pressures of 70 and 90 mbar, which yields injection particle fluxes of 3.5×10^{19} and 4.5×10^{19} particles/s respectively. The experiments were carried out in the standard OP1.1 magnetic configuration using a single and both gas boxes. When injected from both gas boxes neon triggered a radiation collapse that featured a Marfe-like event at the edge and a neutral pressure spike in module 4. The onset of the collapse was caused by the increased plasma density and impurity radiation [28]. Only one discharge with neon injected at 70 mbar reservoir pressure from a single gas box didn't lead to a collapse and it is analysed in the following.

Figure 6 presents an overview plot of the main plasma parameters during this Ne seeding discharge. Time traces of heating power (a), electron temperature (b), electron density (c), bremsstrahlung emission (d) and total radiated power (e) are shown. Heating power from ECRH reaches 2MW after 100 ms and it is kept at this level until the end of the discharge. The gas injection is switched on after 200 ms from the start of the ECRH heating and it lasts for 300 ms. Electron temperature in the core decreases by ~10% during the gas injection, whereas the external channels of the ECE system ($0.82>r/a>0.54$) reveal a drop of 40% of T_e caused by the injected neon. T_e keeps decreasing also after the end of the injection in the whole plasma volume thus meaning a strong impact of neon as radiating away the plasma energy. The line-integrated density increases mainly due to wall outgassing and to some extend also due to the contribution of the electrons coming from the ionization of Ne. Taking the total injected particle number and assuming full ionization and homogeneous distribution along the whole plasma volume the maximum density increase due to Ne would be of 3.5×10^{18} m^{-3}. Hence we conclude that most of the density drive is born again from an uncontrolled neutral source from wall outgassing. Diamagnetic energy reduces by 35% after the injection as an indicator of core degradation. Bremsstrahlung emission is enhanced of a factor 3: considering that n_e increases by a factor 1.6 and core T_e decreases by a factor 0.9 this implies that Z_{eff} increases. Total radiated power increases significantly due to the impurities injection, it keeps raising after the closure of the valve reaching 70% of the input power at 0.58 s.

Figure 7 shows the cooling in the SOL temperature following the neon injection as measured by the limiter Langmuir probes. A significant reduction of 20-30 eV corresponding to a 50% relative reduction is measured by the probes. The temperature continues to lower after the end of the gas injection (see Figure 7b) as measured by the ECE for the confined plasma. This suggests strong recycling of Ne from the limiter surface with consequent radiation and cooling of the plasma after the closure of the valve. Spectroscopic measurements of a Ne I emission line in Figure 8 confirm a large concentration of Ne atoms after the end of the gas injection.

Neon is seen to affect consistently the entire plasma domain, even when injected in small amount, radiating away most of the input power and cooling the plasma from the SOL to the central region. After the end of the gas injection neon continues to radiate, suggesting high recycling. This is consistent with what has been previously observed in LHD where a strong core radiation was measured after stopping the Ne injection. The reason found was the high recycling of neon which gradually enhanced the concentration in the core region [15].
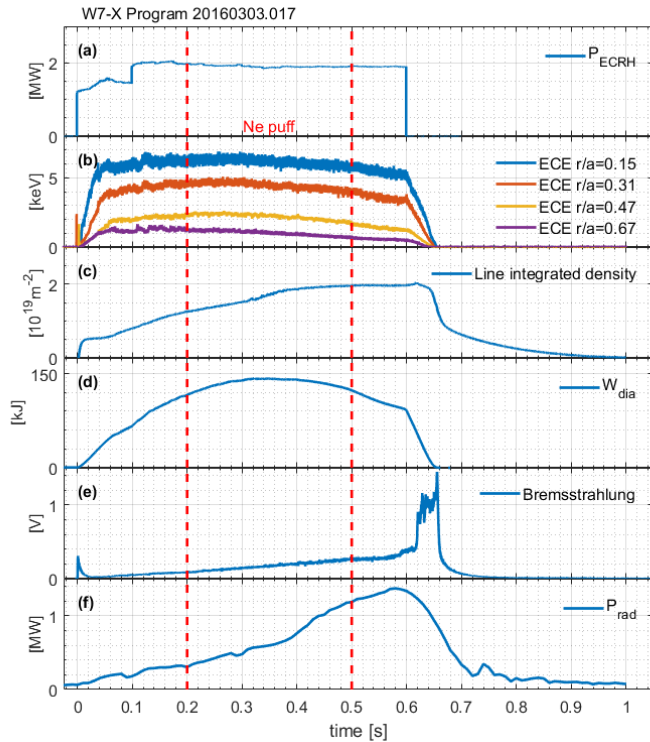

Figure 6. Overview plot of a discharge with Ne gas injection. From top to bottom: (a) ECRH heating power, (b) electron temperature from ECE, (c) line-integrated electron density, (d) diamagnetic energy, (e) bremsstrahlung emission, (f) total radiated power.
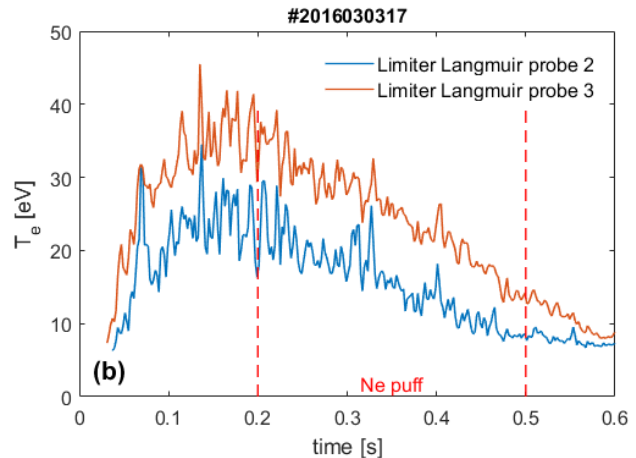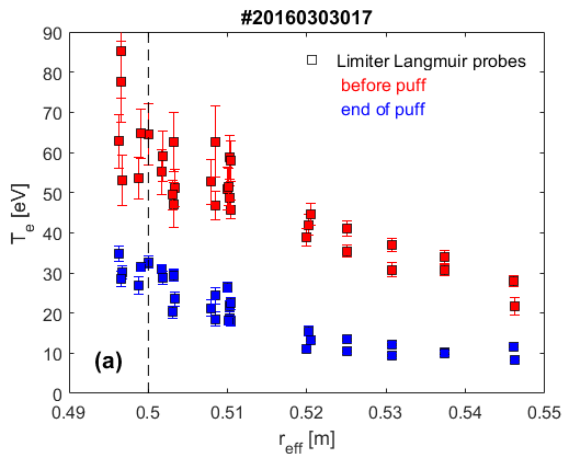
Figure 7. Electron temperatures measured by the limiter Langmuir probes. (a) radial profile before (red) and at the end (blue) of the Ne injection (LCFS is shown as a dashed black line). (b) time traces of two probes from the upper tile array (probe 2 at $r_{eff} = 0.546$ and probe 3 at $r_{eff} = 0.525$).

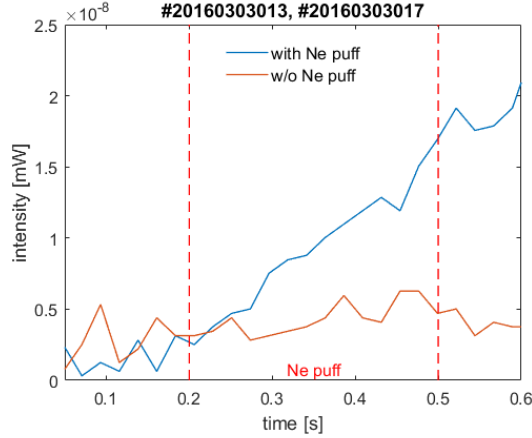**Figure 8.** Line-integrated emissions from Ne I at 430 nm measured by a central line-of-sight spectrometer at $\phi_{tor}=12.3°$.

Analysis of radiation distribution

Nitrogen injection

The radiated power is calculated from LoS-integrated measurements of the horizontal bolometer camera [29]. In Figure 9 the time trace of the total radiated power during a N_2 injection with pulsed gas puff is shown. During stationary plasma phases the radiative power loss fraction P_{rad}/P_{ECRH} is around 25%. With the introduction of nitrogen this fraction raises up to 40%. Every time the valve closes, the radiation immediately drops, the small delay being due to the valve opening time. The radiation decreases with a time constant of ~ 35 ms, thus indicating small recycling and penetration of nitrogen impurities in the confinement region that would keep the level of radiation constantly high after the closure of the valve.

2D emissivity distributions have been obtained using a Bayesian tomographic method based on the bolometer measurements. This method uses Gaussian processes to model the emission distribution and then uses Bayesian inference to calculate a posterior Gaussian process describing the range of possible tomographic reconstructions given the data and model assumptions [30]. The tomographic inversions have been done in the Minerva framework [31].

Figure 10 shows the 2D emissivity distributions for the pulsed N_2 injection discharge at different times. In Figure 11 the radial profiles of the radiated emissivity are also shown. Before the injection the radiation comes from a broad region located inside the confined region with the peak value at $r/a=0.8$. This radiation is mainly emitted by low-Z impurities such as C and O [29]. During the N_2 injection the radiation peak moves outwards at $r/a=0.9$. Nitrogen seems to radiate more outwards with respect to intrinsic impurities. Moreover the radiating layer becomes more strongly localized in the lower part of the cross-section. The bolometer array is very close to the injection point in module 3 and the flux tube which is directly fuelled by nitrogen lies at the bottom of the cross-section measured by the bolometer lines-of-sight (see Figure 1). This could explain why during the gas injection the radiation is concentrated in a region at the bottom of the poloidal section. This shows that the cooling is localized and connected to the injection bundle. Hence, it confirms that the strong limiter cooling seen with the temperature diagnostics is very likely due to a build-up of a residual N source on the limiter due to sticking, and not because of a dominant global cooling that would have led to a homogeneous distribution of the radiated power emissivity.

Neon injection

2D emissivity distributions and corresponding radial profiles have been computed also for the neon seeded discharge presented before and are depicted in Figure 12 and Figure 13. Before the gas injection, the radiation layer is broadly distributed in the outer confined region with a peak value at r/a=0.8 as previously discussed. During the neon injection, the radiation zone shrinks and peaks at r/a=0.9. After the end of the gas injection the radiation belt is still present in the same position with similar high intensity as during the gas injection. This result suggests that neon tends to accumulate in the plasma and it recycles on the wall surfaces without any significant exhaust from the system, keeping the level of radiation high after the end of the gas injection. This is also a reasonable assumption given that the exhaust efficiency of the turbo-molecular pumps for Ne is small. Hence, the injected gas is not exhausted and is continuously available for repetitive cooling after recycling. N_2 in contrast has a lower recycling coefficient due to its sticking and hence is effectively exhausted on the time scales of the discharge by attachment the wall surfaces and hence it is not available as much for repetitive cooling.

The observation that the radiation belt is more poloidally symmetric than in the nitrogen case can be addressed through several hypothesis. The first is that neon is injected into the chamber from the gas box which is located 168° toroidally away from the bolometer array: neon impurities travel a longer distance than nitrogen before reaching the bolometer and hence they can redistribute in the neighbouring flux tubes. The second is the limited numbers of diagnostic channels available for the tomographic reconstruction for this discharge. This necessitates a stronger constrain of symmetry within a flux surface imposed in the tomographic algorithm. Last but not least, the process of recycling and repetitive cooling of neon described before yields a stronger global distribution of the Ne which further reduces the localization effect.
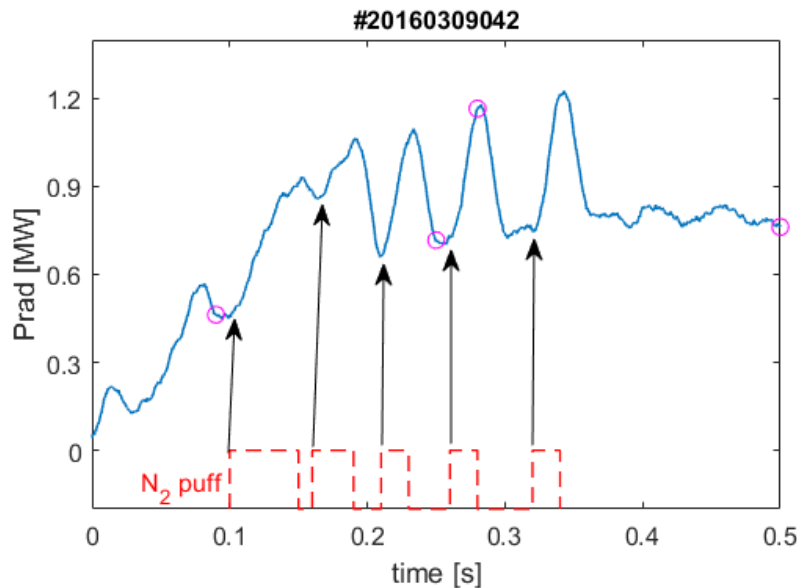

Figure 9. Time traces of the total radiated power measured by the bolometer for a pulsed N_2 injection. Black arrows relate the enhancement of the radiation to the opening of the valve. Magenta circles mark the times at which the emissivity tomographic reconstruction has been calculated.
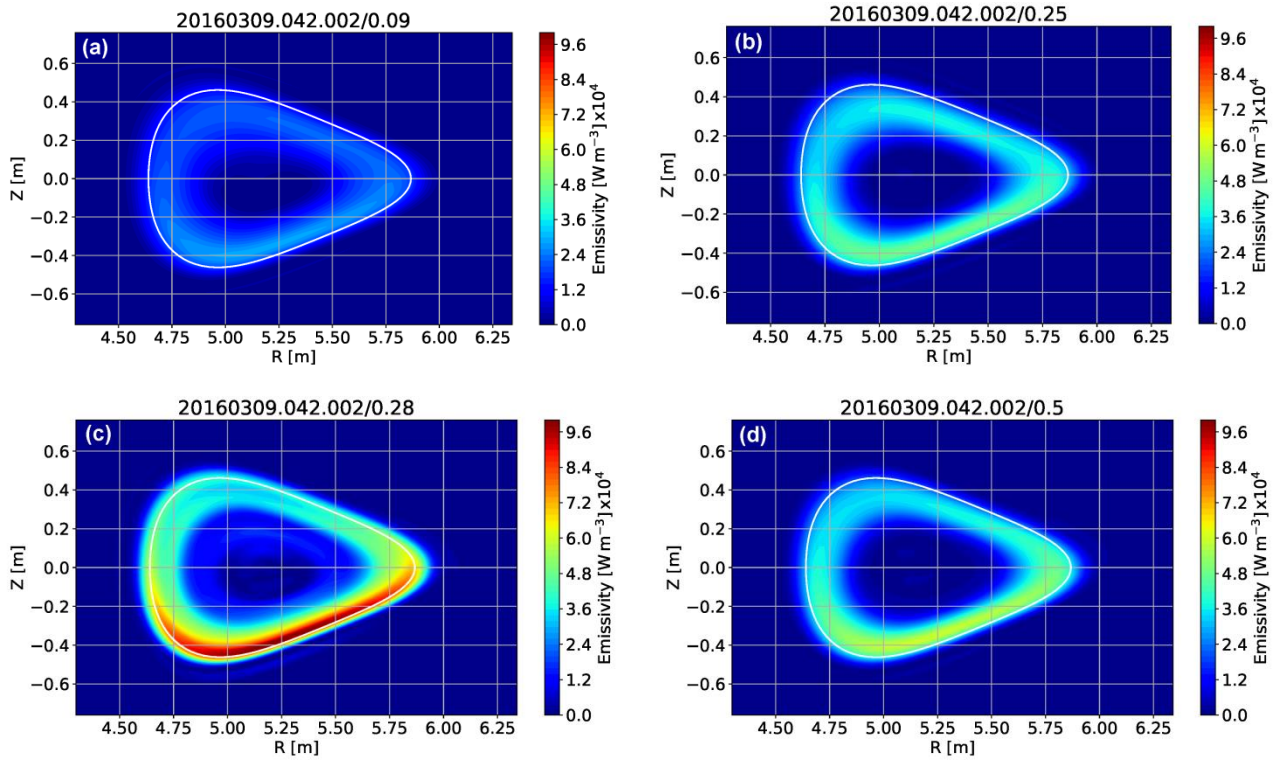
Figure 10. Tomographic reconstruction of the radiated power emissivity in a N_2 seeded discharge with pulsed gas injection. From top left: (a) before the injection (0.09 s), (b) with closed valve (0.25 s), (c) with open valve (0.28 s), (d) after the injection (0.5 s). LCFS is shown in white.
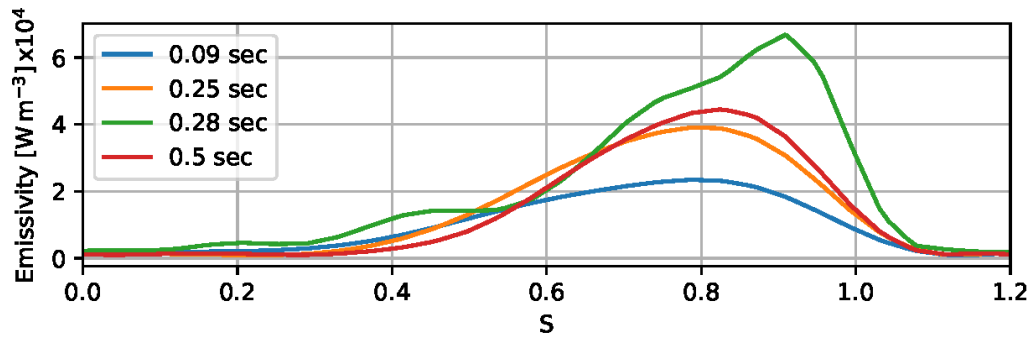

Figure 11. Radial distribution of the radiated emissivity in a N_2 seeded discharge with pulsed gas injection at different times: before the injection (0.09 s), with closed valve (0.25 s), with open valve (0.28 s), after the injection (0.5 s).
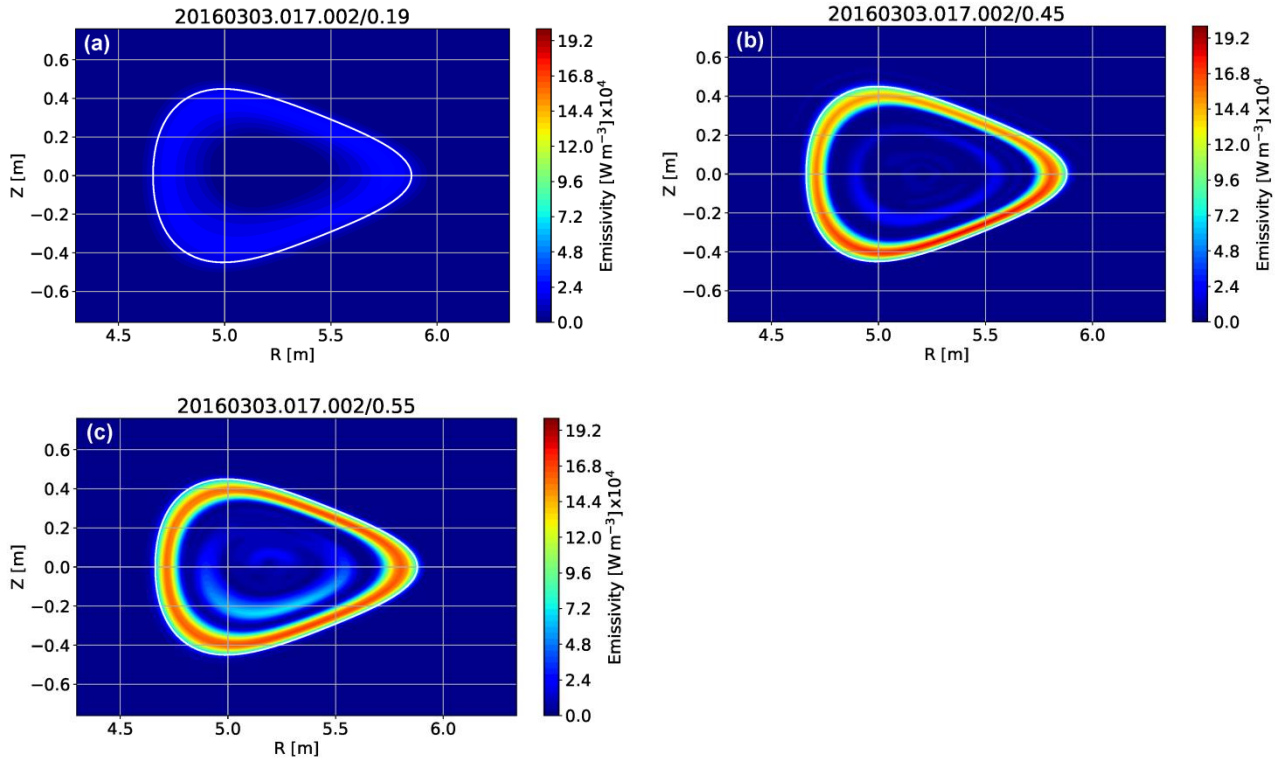
Figure 12. Tomographic reconstruction of the radiated power emissivity in a Ne seeded discharge. From top left: (a) before the injection (0.19 s), (b) during the injection (0.45 s), (c) after the injection (0.55 s). LCFS is shown in white.
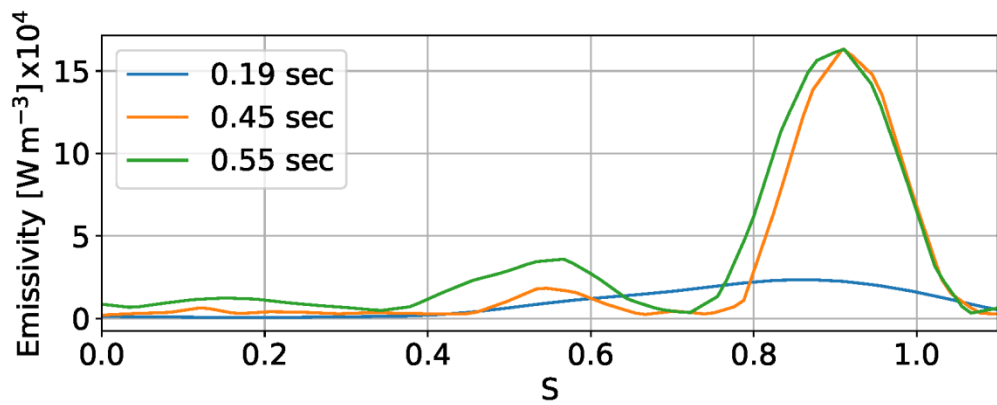

Figure 13. Radial distribution of the radiated emissivity before (0.19s), during (0.45s) and after (0.55s) a Ne seeded discharge.

Analysis of limiter heat fluxes

Heat flux densities on limiter 5 are computed from measurements of the limiter surface temperature acquired with an infrared camera. Figure 14 shows the impact of the nitrogen seeding through the discharge-to-discharge evolution of the average heat flux densities on three different tiles. A clear impact of the seeding is visible in the reduction of the heat flux density with increasing number of N_2 seeded discharges. Consecutive N_2 seeded

discharges increase the global N concentration in the device leading to an enhanced mitigation of the heat load on the limiters. This heat load reduction lasts for the following shots with no N injection, indicating the presence of substantial remaining N in the device. This N legacy effect was already observed in other C-wall devices such as JET [32] and we have discussed in some depth before already. A possible explanation for the N lasting for a long time in the vessel is surface dilution of the PFC material by nitrogen leading either to N-containing layers or to nitride formation [33]. He-cleaning discharges were performed in between the experimental sequence and led to the removal of the N deposited on the wall and to the reestablishment of the wall conditions prior to the N_2 injections. Visible spectroscopy confirms the nitrogen legacy by the prolonged appearance of a nitrogen source over several discharges without active nitrogen seeding, measured in situ by N I and N II lines. The spectra were taken with a visible spectrometer observing the inner wall through a single line-of-sight along the mid-plane. Figure 15 shows the discharge evolution of C III (465 nm) and N II (500.5 nm) for a series of N seeded shots followed by some shots without N injection. A high level of N has been observed to last for the consecutive discharges after the N seeded shots until a series of He cleaning discharges is performed. At the same time a diminishing level of C radiation is measured during the active seeding; this is suggestive of a reduced C sputtering owing to the lower energy of the impinging ions due to plasma cooling and dilution of the layer surface with impinging nitrogen [33]. C sputtering seems to increase again when the active seeding is stopped as indicated by the enhancement in the C line radiation.
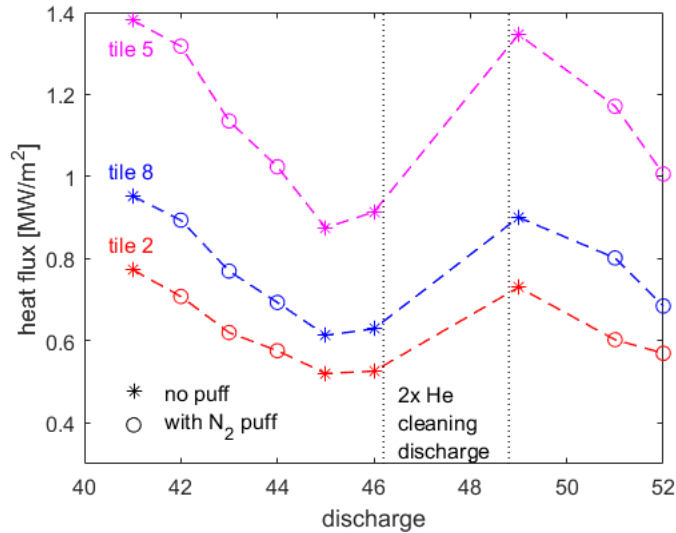

Figure 14. Discharge-to-discharge evolution of the heat flux density on different tiles of limiter 5. The heat flux densities are averaged over the tile surface and over a 200 ms time window.
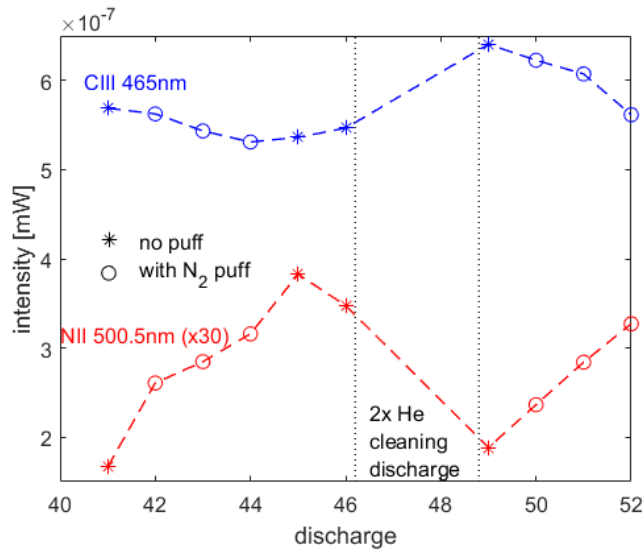
Figure 15. Discharge-to-discharge evolution of C III (465 nm) and N II (500.5 nm) averaged over 200 ms. Measurements from a central line-of-sight spectrometer at $\phi_{tor}=12.3°$.

Modelling results

A first systematic numerical assessment of plasma edge transport processes in the limiter configuration of W7-X has been presented in [16]. In this reference, the transport of intrinsic (C) and extrinsic (Ne and N) impurities in the SOL and their impact on the power balance and limiter heat fluxes was numerically assessed. The fully 3D coupled fluid plasma edge transport and kinetic neutral transport Monte Carlo code EMC3-EIRENE was used in this study [34][35].

These predictive studies were revised in order to compare 3D modeling with the experimental findings presented here. The numerical assessment is targeted on the basic effects of power losses based on input parameters adjusted towards the typical conditions of discharges presented. Since the 3D model solves the plasma fluid and kinetic transport equations in steady state conditions an average edge density value of $n_e \sim 4\times10^{18}$ m^{-3} is chosen. The heating power is set to $P_{in} = 2$ MW. Anomalous perpendicular transport for particles is estimated to be $D_\perp = 0.5$ m^2 s^{-1} and for energy a typical relation of $\chi_\perp = 3D_\perp$ is used. The impact of intrinsic impurity and seeded impurity sources will be discussed with respect to the distribution of radiated power and impact on SOL temperatures. The resulting integrated heat fluxes decrease with enhanced fractional power losses of $f_{rad}=P_{rad}/P_{in}$. The cooling effects within the edge are discussed based on radial T_e profiles.

Initially, a modeling solution for clean reference plasma was obtained based on these input parameters. In a second step, the effects of intrinsic losses by the sputtered C are considered. According to an assumption based on bolometer analysis [29], carbon and oxygen are suspected to be the main edge radiators. Fractional power losses of $f_{rad}=25\%$ (0.5 MW) are set as boundary conditions treating the limiter as main erosion and outgassing source for both impurity species. The calculations yield impurity fluxes of $\Gamma_C = 2.8\times10^{21}$ s^{-1} and $\Gamma_O = 1.4e\times10^{21}$ s^{-1} for carbon and oxygen, respectively. That is, only half the amount of oxygen is required to achieve the same radiative losses as carbon. An overview of the flux surface averaged total impurity radiation P_{rad} and the electron temperatures T_e is shown in the plots in Figure 16 (a) and (d), respectively. The shape and peak position of carbon (black) and oxygen (blue) radiation distributions are very similar and nearly match with each other within the SOL. With the current assumptions, 16-17% of these radiative losses occur in the SOL while the main radiation is located in the confined region close to the LCFS. Both impurities cause almost the same cooling impact, e.g., measured by a drop of ~22 eV at the LCFS. The temperature losses are more pronounced at the LCFS since P_{rad} is enhanced in this region and $T_e \propto (P_{in} - P_{rad})$.

For the nitrogen seeding experiments, two cases are considered. In the first case, N$_2$ is injected from a remote location setting $f_{rad} = 40\%$ (0.8 MW) neglecting any other impurities and assuming absorption once nitrogen hits

the wall/limiter due to its low recycling properties. The required flux is found to be $\Gamma_N = 6.5\times10^{21}\,s^{-1}$. The resulting P_{rad} and T_e are shown as profiles (blue) in Figure 16 (b) and (e). In the second case, the C background is set as discussed previously and nitrogen is injected in an amount to account for another 25% of additional power losses such that the total loss by intrinsic C and seeded N adds up to $f_{rad} = 50\%$ (1 MW). The carbon and nitrogen fluxes turn out to be $\Gamma_C = 2.6\times10^{21}\,s^{-1}$ and $\Gamma_N = 3.9\times10^{21}\,s^{-1}$.The resulting profiles are shown in red. While the pure nitrogen seeding case shows peaking within the near SOL, the total radiation maximum shifts in case of combining N and C to the LCFS. The temperature profiles in figure (e) show a stronger drop in the case with nitrogen seeding into the SOL. That could be explained by the remote position of the impurity gas source, causing ~56% of the radiation losses to occur within the SOL. The combination of carbon and nitrogen sourced from the limiter and remotely, respectively, causes a more uniform cooling in the near and far SOL (see in (e) the T_e plot in red). This is caused by power losses within the confinement, whereas the SOL accounts for 35.6% of the total losses. In the case of pure N seeding, the T_e drop at the LCFS is only 30% and reaches 40% deeper within the SOL. The position of the effective energy sink can be seen in the temperature profiles by comparing the decay of black, blue and red lines respectively. This analysis shows clearly that the nitrogen alone wouldn't be an effective means for cooling the near SOL without intrinsic radiators, shifting the peak power losses further inwards.

For neon, the procedure is similar but extended by one case. First pure remote neon seeding is assumed with $f_{rad} = 40\%$ (0.8 MW) resulting in a flux of $\Gamma_{Ne} = 2.6\times10^{21}\,s^{-1}$. The neon radiation is shown in plot (c) in Figure 16 as a solid blue line. The peak maximum and main power losses are located within the confinement, with 21.6% of SOL power losses. Due to its high recycling neon is also sourced from the limiter with $f_{rad} = 40\%$ (0.8 MW) corresponding to recycling neon only. Here a reduced flux of $\Gamma_{Ne} = 9.7\times10^{20}\,s^{-1}$ is obtained which corresponds to only 37% of the remotely seeded amount. Results for the Ne modeling are shown by the blue dashed lines for P_{rad} and T_e in the plots (c) and (d) of Figure 16. Neon started as sourced/recycled from the limiter causes a further shift of the dominant radiation as the main volumetric power sink into the confinement, while the SOL losses are only 8.3%. However, the results show that the impurity source location of neon has only a small impact on the cooling effect on edge temperature. The temperature drops scale like (P_{in} - P_{rad}) at the LCFS, and they are in case of remote seeding slightly more effective in the far SOL. In the third case, neon is seeded remotely with $f_{rad} = 40\%$ (0.8 MW) in combination with C sourced from the limiter with $f_{rad} = 25\%$ (0.5 MW) corresponding to a total loss fraction of $f_{rad} = 65\%$ similar to the experimentally measured total losses. The limiter carbon flux and the neon injection rates are in this case $\Gamma_C = 2.3\times10^{21}\,s^{-1}$ and $\Gamma_{Ne} = 1.8\times10^{21}\,s^{-1}$. Each is slightly reduced compared to the above described individual treatments. The resulting profiles are shown in red in the plots (c) and (f) of Figure 16. The SOL power loss fraction is now 14.7%, and the maximum is shifted slightly outwards with respect to the pure neon radiation distributions. With an effective main energy sink mostly located within the confinement, the temperature reduction is uniform and scales like (P_{in} - P_{rad}) in the main SOL.

In conclusion, the results provide some general insights within a set of chosen boundary conditions and assumptions concerning the ideal geometry of the problem. In comparison to the experiment one main deviation is found to be the levels of impurity fluxes. Those are in case of seeding well defined. In the modeling, they tend to be one order of magnitude higher. The lowest flux is obtained in the modeling for neon sourced from the limiter idealizing its recycling properties. The fluxes are lower in the experiment, and radiative power distributions have their maxima a few centimeters deeper within the LCFS compared to the modeling. The modeling provides a potential reason for the shifts of the radiation peak position. Firstly, the cooling potential of the respective impurity determines the effective radial energy sink. It is a function of T_e. The P_{rad} maxima of Ne are shifted further inwards compared to C and N because it radiates at higher T_e. Secondly, if one combines different impurities, such as C and N or C and Ne, they define new effective cooling potentials different from the individual ones. The above results indicate, for example, a reduction of individual impurity fluxes in case of combined treatment. The combination of their nonlinear cooling potentials may make them more effective and cause more homogenous inward shifted radiation. Contributions of other impurities neglected in this modeling may move the radiation further inwards. Furthermore, the modeling indicates that the location and recycling properties matter a lot for the cooling efficiency. Seeding of nitrogen solely released into the far SOL with zero recycling has a smaller effect on temperatures around the LCFS and is more efficient deeper in the SOL. Impurities sourced from the limiter are always more efficient and cause homogeneous SOL cooling. The recycling and source location of the impurities matter for the radial radiation distribution as well. Besides recycling self-sputtering may add an additional uncertainty not yet implemented in the 3D model. In the experiment impurity injection but also general wall

outgassing changed the local and global densities dynamically. In particular local density changes may enhance intrinsic impurity sourcing and radiation as well because of enhanced chemical sputtering. Impurities can also cause enhanced sputtering once injected. Mainly, a better resolution of edge impurity content is required before further benchmarking and refinement of the 3D modeling can be performed.
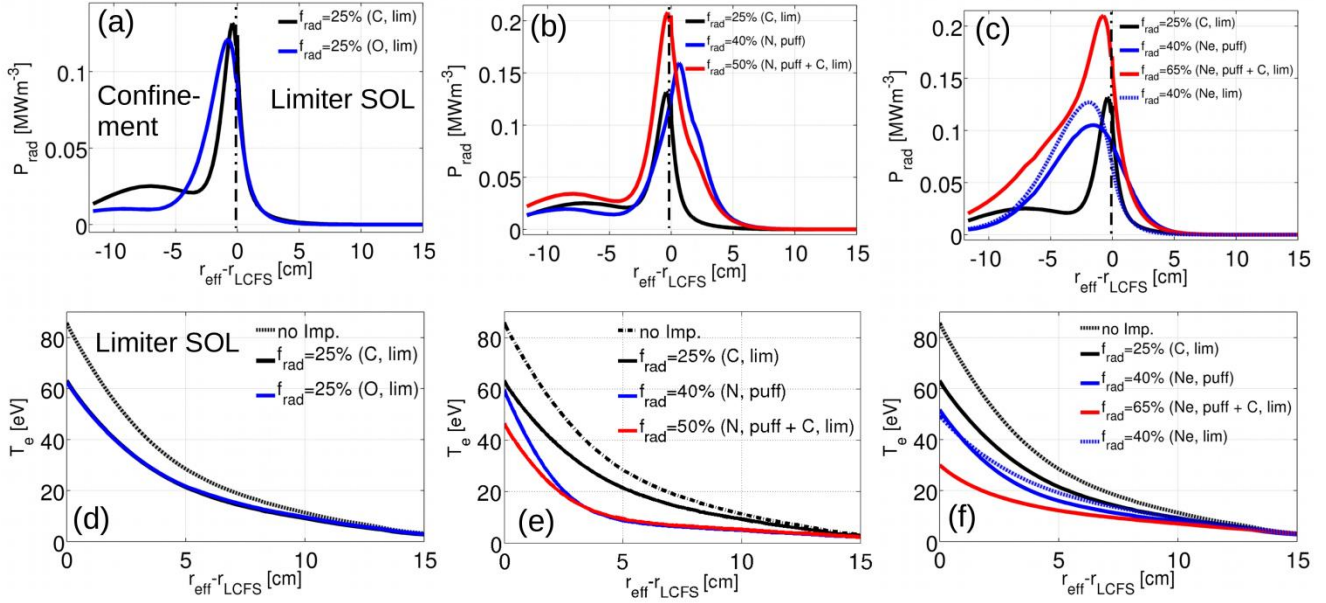

Figure 16. Flux surface averaged radial profiles of radiated emissivity P_{rad} [MW m^{-3}] (top) and T_e (bottom). The vertical dashed lines mark the position of the LCFS in the top plots of P_{rad}. (a) and (d) show resulting profiles for carbon (black) and oxygen (blue) sourced from the limiters. (b) and (e) show carbon sourced from the limiter (black), nitrogen injected (blue) and combination of carbon sourced from the limiter and nitrogen injected (red). (c) and (f) show carbon sourced from the limiters (black), neon injected (blue), combination of carbon and neon, both sourced from the limiter (red) and case of neon sourced from the limiters (dashed blue). The T_e profiles of the plasma without impurities is shown in (f) for reference (dashed black).

Summary and Conclusions

In this work the first radiative edge cooling experiments on Wendelstein 7-X limiter start-up phase have been presented, together with a 3D modelling of these experiments with EMC3-EIRENE. Injections of nitrogen and neon were carried out from two gas boxes in two toroidal positions and the effects on the edge temperature, radiated power and heat loads on the limiter were observed. A set of three edge temperature diagnostics located in different positions within the SOL allows to characterize the nature of the cooling, discerning local vs. global cooling. The bolometer diagnostic provides insight into the radial position of the radiation layer and to the extent possible by the spatial resolution of the system also into the poloidal structure of the radiation. An infrared camera looking at the limiter gives information about the mitigation of the heat loads on the limiter tiles.

Injection of nitrogen impurities in the edge of the plasma leads to a reduction of the electron temperature in the SOL and to a mitigation of the heat load on the limiters. The temperature decrease is not uniform in the SOL, in particular it is found that cooling at the downstream limiter position is stronger than local upstream cooling in the same flux tube that is fuelled by the gas valve. This is due to cross field transport into the limiter flux tubes, followed by N_2 accumulation and generation of a local source at the limiter surface. Nitrogen has been shown to be a good choice for short pulse cooling: variations of temperature and radiated power are fast correlated with the opening/closing of the gas valve. Both react quickly with the gas being injected in and in the same way they restore soon after the valve closing. This is very promising for the foreseen feedback-controlled gas injection being implemented for the next divertor campaigns.

Neon has been also analysed, which has different physical properties, in particular it has a larger number of radiating energy levels and a high recycling from carbon surfaces. Neon is injected with a particle influx in the ratio of 1/3 with respect to atomic nitrogen, providing under comparable plasma conditions a similar cooling in the SOL but a higher radiated power. The cooling extends also in the confined region leading to a degradation of the discharge. Moreover the radiation and the consequent cooling continue after the end of the gas injection indicating strong accumulation and recycling.

Comparison of these key experimental observations with EMC3-EIRENE resulted in qualitative agreement on the main trends. In particular the ratio of the impurity influxes between the two species to reach the same radiated power level was seen as well as the localization of the radiated power from the injected gas species and the relative temperature reduction. Also, the recycling properties of Ne vs. N were qualitatively recovered and support the significantly different behaviour and hence quite different utilization opportunities of these two gas species for radiative edge cooling. Nevertheless some aspects are still not implemented in the code, such as combination of cooling potentials from different species, contribution of heavier impurities and self sputtering. They presently prevent reproducing quantitatively the experiment results. This is an important point for enhancement of the modelling approach, which was identified by this study.

These experiments served as an important guideline for the next divertor campaigns. For those will be crucial to identify a proper way to execute radiative edge cooling experiments in order to both mitigate the heat loads on the plasma facing components and facilitate the transition to the detachment regime. In this regard extensive experiments are planned to be carried out in the new divertor configuration campaigns, using both N and Ne but also Ar (in later high performance operation/H-mode also Kr or Xe).

References
[1] Wolf R *et al* 2017 *Nucl. Fusion* 57 102020
[2] Klinger T *et al* 2017 *Plasma Phys. Control. Fusion* **59** 014018
[3] Bozhenkov S, Effenberg F, Feng Y, Geiger J, Hartmann D A, Hölbe H, Pedersen T S and Wolf R C 2014 *41st EPS Conf. on Plasma Physics* P1.080
[4] König R *et al* 2015 *J. Instrum.* **10** P10002
[5] Pedersen T S *et al* 2015 *Nucl. Fusion* **55** 126001
[6] Krychowiak M *et al* 2016 *Rev. Sci. Instrum.* **87** 11D304
[7] Geiger J *et al* 2013 *Plasma Phys. Control. Fusion* **55** 014006
[8] Hölbe H, Pedersen T S, Geiger J, Bozhenkov S, König R, Feng Y, Lore J and Lumsdaine A 2016 *Nucl. Fusion* **56** 026015
[9] Maddison G P *et al* 2011 *Nucl. Fusion* **51** 042001
[10] Wang H Q *et al* 2016 *58th Annual Meeting of the APS Division of Plasma Physics*
[11] Reinke M L, Hughes J W, Loarte A, Brunner D, Hutchinson I H, LaBombard B, Payne J and Terry J L 2011 *J. Nucl. Mater.* **415** S340–4
[12] Kallenbach A *et al* 2010 *Plasma Phys. Control. Fusion* **52** 055002
[13] Mukai K *et al* 2015 *Nucl. Fusion* **55** 083016
[14] Tanaka H *et al* 2016 *Nuclear Materials and Energy* **12** 241-246
[15] Morisaki T *et al* 2015 *J. Nucl. Mater.* **463** 640–643
[16] Effenberg F *et al* 2017 *Nucl. Fusion* **57** 036021
[17] Winters V *et al* 2017 *Phys. Scr.* **2017** T170
[18] Barbui T, Krychowiak M, König R, Schmitz O, Muñoz Burgos J M, Schweer B and Terra A 2016 *Rev. Sci. Instrum.* **87** 11E554
[19] Bosch H-S *et al* 2013 *Nucl. Fusion* **53** 126001
[20] Renner H *et al* 2000 *Nucl. Fusion* **40** 1083

[21] Renner H *et al* 1993 *20th EPS Conf. on Plasma Physics*

[22] Stephey L *et al* 2018 *Physics of Plasmas* **25** 062501

[23] Griener M *et al* 2017 *Rev. Sci. Instrum.* **88** 033509

[24] Schweer B, Brix M and Lehnen M 1999 *J. Nucl. Mater.* **266** 673-678

[25] Drews P *et al* 2017 *Nucl. Fusion* **57** 126020

[26] Niemann H, Jakubowski M, Pedersen T S, König R, Wurden G A, Effenberg F and Zhang D 2016 *43rd EPS Conf. on Plasma Physics* P4.005

[27] Zhang D *et al* 2010 *Rev. Sci. Instrum.* **81** 10E134

[28] Wenzel U *et al* 2018 *Nucl. Fusion* **58** 096025

[29] Zhang D *et al* 2016 *43rd EPS Conf. on Plasma Physics* P4.015

[30] Svensson J 2011 *JET Internal Report* EFDA-JET-PR(11)24

[31] Svensson J and Werner A 2007 *IEEE Int. Symp. on Intelligent Signal Processing* pp 1–6

[32] Brezinsek S *et al* 2011 Nucl. Fusion **51** 073007

[33] Brezinsek S, Jachmich S, Rapp J, Meigs A G, Nicholas C, O'Mullane M and Pospieszczyk A 2011 *J. Nucl. Mater.* **417** 624–628

[34] Feng Y, Sardei F, Kisslinger J, Grigull P, McCormick K and Reiter D *Contrib. Plasma Phys.* 2004 **44** 57–69

[35] Feng Y *et al* 2014 *Contrib. Plasma Phys.* **54** 426–431